Subterahertz filtering six-port junction

Chen, Xun; Salek, Milan; Zhang, Qingfeng; Wang, Yi

DOI:
10.1109/TMTT.2022.3186322

Subterahertz Filtering Six-Port Junction

Xun Chen, Milan Salek, Qingfeng Zhang, *Senior Member, IEEE,* Yi Wang, *Senior Member, IEEE,*

***Abstract*—This paper presents a D-band E-plane 90° filtering coupler and a D-band six-port junction (SPJ), both working at 150 GHz. The coupler is formed by ten resonators, having a fourth-order Chebyshev response. Two of the couplers were combined with a 90° 3-dB branch-line coupler to build the filtering SPJ with twenty resonators in total. Inheriting from the filtering coupler, the SPJ also has a fourth-order Chebyshev response. A coupling matrix (CM) consisting of both resonant and non-resonant nodes, based on the coupling topology, was constructed to predict the theoretical responses. Guided by this coupling matrix, the coupler and the SPJ were designed and modelled. In addition, two silicon-based absorber chips were designed and implemented as two matched loads in the filtering SPJ. The SPJ was optimized, fabricated and tested. The center frequency of the SPJ is 150 GHz and the bandwidth is 4 GHz. Simulation shows 0.5 to 0.7 dB insertion loss at 150 GHz and maximum 3° phase error in the working band. The measurement gives the same center frequency and bandwidth. The response shows 0.7 to 2.0 dB insertion loss at 150 GHz and maximum 15° phase error in the working band.**

***Index Terms*— coupling matrix, filtering coupler, non-resonant structure, six-port junction, subterahertz.**

I. Introduction

THE SIX-PORT concept was initially used in the measurement of phase and instantaneous frequency in [1]. It was extended to measurement of both magnitude and phase of a device-under-test (DUT) in [2]. With the increasing demand for low loss, low complexity and cost-effectiveness, six-port junctions (SPJs) have been extended to receivers to replace conventional mixers [3]. Lots of works have dedicated to the design and application of SPJs [4]-[7]. The principle of SPJ in homodyne and heterodyne receivers was detailed in [4], while [5] provided a thorough review. Two input signals, one from the RF antenna and the other from the local oscillator are summed up in the SPJ. The output signals are the superpositions and are converted directed to the baseband by the diodes (power detectors). After that, these signals are amplified and filtered for further processing. The decoder transfers the four signals to the I/Q signal for demodulating. [6] and [7] presented two SPJ realizations, one based on substrate integrated waveguide (SIW) [6] whereas the other on dually polarized waveguide [7]. The growing demand on bandwidth [8] drives the development of millimeter wave (MMW) devices including SPJs. Among the MMW frequency bands, D-band (110 – 170 GHz) is particularly attractive for wireless communications, earth-observation/remote-sensing, and high-resolution radars, as it contains the atmospheric window where the propagation loss is relatively low [9]. However, the design and implementation of devices at high frequencies (100 GHz plus) is very challenging, as the radiation loss and substrate loss are strong and the requirement for manufacture accuracy is high. Passive devices such as couplers and filters working in or above D-band have been reported in [10] – [17]. When minimum loss is the design drive, computer numerical control (CNC) machined waveguides are usually used.

Another source of losses, for waveguide components especially at subterahertz frequencies, is the flange interconnection between them. A technique to circumvent this is the so-called functionally integrated passive devices, where multiple circuit functions are merged into one device avoiding component cascading or interconnection. This also leads to miniaturization. For example, a dual band filtering coupler using two types of resonators was reported in [18]. A filtering power divider was given in [19]. Besides, filtering antennas also attracted great attention [20] – [22].

Previously we have reported a filtering SPJ working in X-band [23] that consists of two 180° filtering couplers, one 180° branch-line and one 90° branch-line coupler. The 180° branch-line coupler was formed by a 90° branch-line coupler with additional phase shifting feature as reported in [24]. This configuration requires slopes in the waveguides, which is impractical for D-band CNC machining. To overcome this, a novel 90° resonator-based filtering coupler were proposed and used in this D-band filtering SPJ design. There have been some works on resonator-based filtering couplers [25]-[27], but all of them are 180° couplers. Resonator-based 90° filtering hybrids are much more difficult to implement. To achieve the 90° phase, one additional coupling (along with one additional resonator) is needed along one of the two output paths. This causes unbalanced responses of the two outputs and undesired out-of-band poles. A 90° filtering coupler was shown in [28], using coupled lines. This structure is too complicated to be extended to designs with other transmission media, as compared with resonant structures. In the proposed 90° filtering coupler, there are ten resonators, two of which act as power splitters, which avoids the side effect brought by the additional resonator. The ten resonators give the coupler a fourth-order

X. Chen and Q. Zhang are with the Department of Electrical and Electronic Engineering, Southern University of Science and Technology, Shenzhen 518055, China (e-mail: zhang.qf@sustech.edu.cn).

X. Chen, M. Salek and Y. Wang are with the School of Electrical, Electronic and Systems Engineering, The University of Birmingham, Birmingham B15 2TT, U.K. (e-mail: Y.Wang.1@bham.ac.uk).

The work was supported by the U.K. Engineering and Physical Science Research Council (EPSRC) under Contract EP/P020615/1 and EP/S013113/1 and supported by GuangDong Basic and Applied Basic Research Foundation (2021B1515120029), and Shenzhen STIC funds (JCYJ20190809115419425). (Corresponding author: Yi Wang and Qingfeng Zhang.).

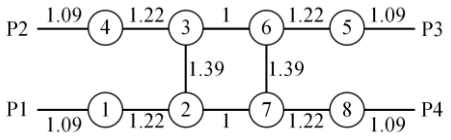

Fig. 1. Topology of a 90° filtering coupler

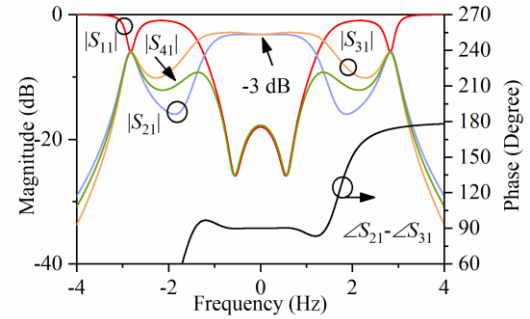

Fig. 2. The magnitude response and phase response of the 90° filtering coupler shown in Fig. 1, showing spurious transmission poles.

Chebyshev filtering response. Using this coupler, a D-band filtering SPJ will be presented. Unlike the conventional SPJ, normally built by three 90° 3-dB couplers and one 3-dB power divider [6], the proposed SPJ comprises twenty resonators and one 90° 3-dB coupler. A coupling matrix (CM) that combines both resonant and non-resonant structures [23] was also built, to predict the theoretical response. In addition, a simple and compact silicon-based absorber has been designed and implemented as the waveguide termination load. The topology was realized in a commercial full-wave simulation software (CST) and fabricated. This passive junction is part of an alternative D-band receiver module for radar and communication applications.

II. E-Plane 90° Filtering Coupler

A. Topology and the Ideal Response

By replacing the transmission lines in conventional branch-line 90° filtering couplers with resonator couplings, a resonator-based 90° coupler can be obtained as shown in Fig. 1. P1 is the input port, P2 and P3 are two outputs while P4 is isolated. Clearly, there will be a 90° phase shift between P2 and P3 due to the extra coupling in resonator 3 and 6. The number of resonators is also different in the two output paths from P1 to P2 and P3. In the path of P1 to P2, there are resonator 1, 2, 3 and 4 whereas in the path of P1 to P3, the available resonators are 1, 2, 3, 6 and 5. This causes unbalanced response of $|S_{21}|$ and $|S_{31}|$. According to the coupling values given in Fig. 1, the magnitude and phase responses were derived and shown in Fig. 2. It can be noticed that between -1 to 1 Hz, the filtering coupler functions properly. However, around -3 and 3 Hz, there are two unwanted poles. The poles cannot be moved into the working band nor cancelled as the two output paths are different in the number of resonators. To overcome this problem, resonators 3 and 6 must act as two non-resonant power splitters. Fig. 1 was therefore modified, and a new 90° filtering hybrid was proposed in Fig. 3.

There are ten resonators in total. The topology is symmetric with respect to line AA'. When input from Port 1, Port 3 and Port 4 are two outputs while Port 2 is isolated. When input from Port 3, Port 1 and Port 2 are two outputs and Port 4 is the isolation port. In the topology, Resonator 9 and 10 act as two power splitters but resonators, achieved by large values (larger than 5) of m_4, m_5 and m_{p2}. The optimized coupling values for this topology are given in (1).

$$\begin{cases} m_1 = 0.699 \\ m_2 = 0.912 \\ m_3 = 1.080 \\ m_4 = 33.32 \\ m_5 = 8.48 \end{cases} \quad \begin{matrix} m_{P1} = 1.038 \\ m_{P2} = 5.755 \end{matrix} \tag{1}$$

The aimed working bandwidth is 4 GHz and the center frequency is 150 GHz. Thus, the fractional bandwidth is 0.0267. Converting the couplings and external q from normalized to real frequency domain, there are:

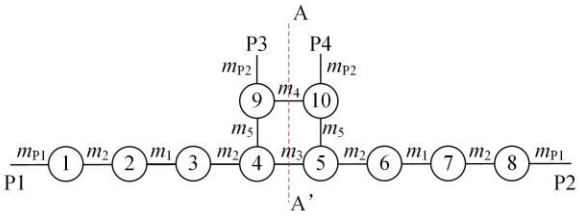

Fig. 3. Topology of the proposed 90° filtering coupler.

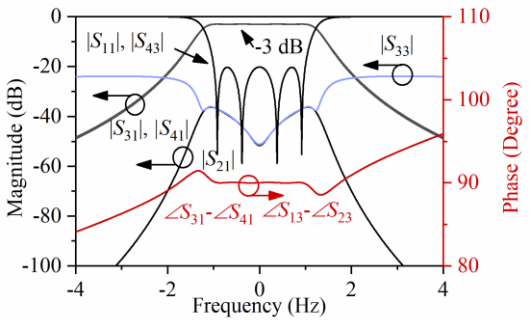

Fig. 4. Magnitude and phase response of the proposed filtering coupler from the coupling values given in (1).

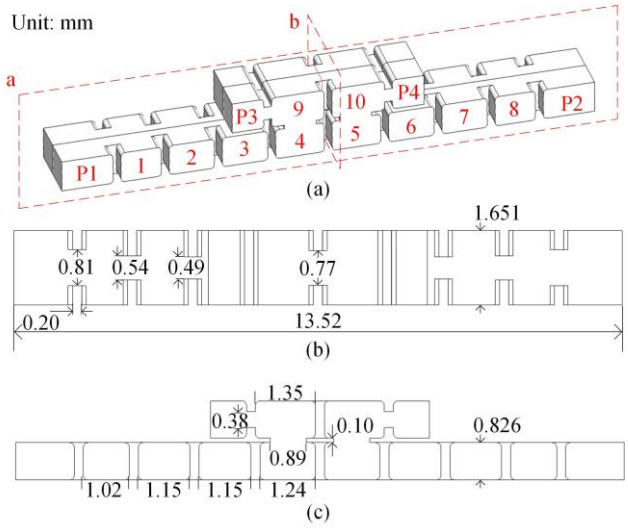

Fig. 5. Air model of the D-band E-plane filtering coupler. (a) The overall view. (b) The top view. (c) The front view. The index of resonators and ports are depicted in red.

$$\begin{cases} M_1 = 0.0186 \\ M_2 = 0.0243 \\ M_3 = 0.0287 \\ M_4 = 0.886 \\ M_5 = 0.226 \end{cases} \quad \begin{matrix} Q_{ex1} = 34.89 \\ Q_{ex2} = 1.135 \end{matrix} \tag{2}$$

These couplings are for an ideal response but some of the values (e.g. M_4, M_5, Q_{ex2}) are difficult to achieve in practice. Compromise was made in the physical model design as discussed later. According to (1), the theoretical magnitude response of the filtering coupler is given in Fig. 4. $|S_{11}|$ and $|S_{43}|$ overlap each other, giving a fourth-order Chebyshev response. Over the pass band, $|S_{33}|$ and $|S_{21}|$ are both lower than – 20 dB. Due to symmetry, input from Port 1/2 or Port 3/4 will be split into halves at Port 3 and 4 or Port 1 and 2, respectively. Fig. 4 also gives the phase response of the filtering coupler. In the working band, the phase difference is 90° between the two outputs.

B. Realization of the D-Band E-Plane Filtering Coupler

The filtering coupler was realized in rectangular cavity resonators, as shown in Fig. 5. To achieve the E-plane structure, Resonator 9 and 10 were placed upon Resonator 4 and 5. The whole coupler is symmetrical with respect to Plane a and b, depicted in red dash lines. Fig. 5(b) and Fig. 5(c) give the dimensions. The internal corners were rounded by 0.1 mm in radius to meet the requirements of CNC machining. Note the irises between resonator 9 and Port 3, resonator 10 and Port 4 are capacitive in order to obtain large external coupling m_{p2}.

C. Simulated Response

As mentioned earlier, the coupling values associated with Resonator 9 and 10 (m_4, m_5, m_{P2} or M_4, M_5, Q_{ex2}) are difficult to implement. Optimization has been applied to the simulation. The realized couplings in the physical model are given in (3).

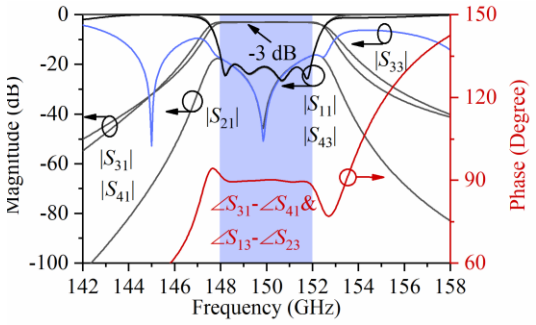

Fig. 6. Simulated magnitude response and phase response of the D-band E-plane filtering coupler.

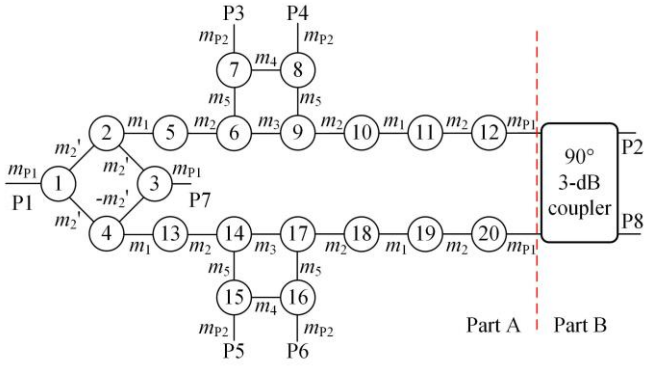

Fig. 7. Topology of the proposed filtering SPJ. Part A is formed by two identical filtering coupler and Part B is a 90° 3-dB coupler.

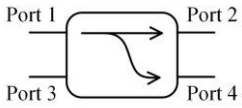

Fig. 8. 90° 3-dB coupler.

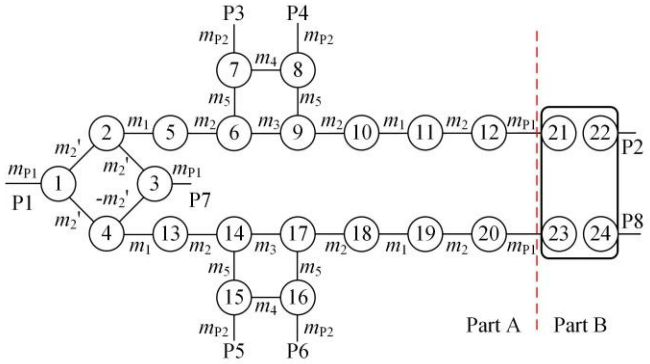

Fig. 9. Topology of the proposed filtering SPJ with the 90° 3-dB coupler represented by nodes 21, 22, 23 and 24.

$$\begin{cases} M_1^r = 0.0190 \\ M_2^r = 0.0263 \\ M_3^r = 0.0270 \\ M_4^r = 0.0961 \\ M_5^r = 0.0670 \end{cases} \quad \begin{matrix} Q_{ex1}^r = 29.49 \\ Q_{ex2}^r = 10.29 \end{matrix} \tag{3}$$

The simulated response can be found in Fig. 6. In the working band (148 – 152 GHz), $|S_{11}|$ and $|S_{43}|$ are lower than -20 dB, $|S_{33}|$ and $|S_{21}|$ are lower than -17 dB. The maximum magnitude imbalance in the working band is 0.34 dB and the maximum phase error is 2°. Within the passband, the simulated performance agrees with the theoretical one from the coupling matrix very well. The simulated 90° filtering coupler model was used in the design of the filtering SPJ later.

III. E-Plane Filtering SPJ

A. Topology

Conventional SPJs consist of three 90° 3-dB couplers and one 3-dB power divider [6]. In this work, the E-plane filtering 90° coupler described in Section II has been used in the filtering SPJ. Two identical filtering couplers were combined by sharing Resonator 1 and 3 (Fig. 7). The combined couplers are labelled "Part A". By adding a 90° 3-dB coupler (Part B), a filtering SPJ can be built (Fig. 7). The coupling between resonator 3 and 4 is negative while others are positive. Its coupling is deduced by:

$$m_2' = m_2 / \sqrt{2} \tag{4}$$

In the SPJ, Port 1 is one input port while Port 2 is the other. Port 3, 4, 5 and 6 are the four outputs. Port 7 and Port 8 are supposed to be terminated by matched loaded. When input from Port 1, the signal is split into halves to the upper and lower filtering coupler, with no phase shift. Then at Port 3 and Port 4, Port 5 and Port 6, the outputs have 90° phase shift. When input from Port 2, the signal will also be split into halves, but with 90° phase shift. The theoretical phase shifts at the four outputs are therefore:

$$
\begin{cases}
m_{P1,1} = m_{P7,3} = m_{12,21} = m_{20,23} = 1.038 \\
m_{p2,22} = m_{p8,24} = 1 \\
m_{p3,7} = m_{p4,8} = m_{p5,15} = m_{p6,16} = 5.755 \\
m_{1,2} = m_{2,3} = -m_{3,4} = m_{1,4} = 0.645 \\
m_{2,5} = m_{4,13} = m_{10,11} = m_{18,19} = 0.699 \\
m_{5,6} = m_{9,10} = m_{11,12} = m_{13,14} = m_{17,18} = m_{19,20} = 0.912 \\
m_{6,9} = m_{14,17} = 1.080 \\
m_{6,7} = m_{8,9} = m_{14,15} = m_{16,17} = 8.48 \\
m_{7,8} = m_{15,16} = 33.32 \\
m_{21,22} = m_{23,24} = j\sec 2\theta \times \sqrt{2}\cos\theta \\
m_{21,23} = m_{22,24} = j\sec 2\theta \\
m_{21,24} = m_{22,23} = -j\sec 2\theta \times \sqrt{2}\sin\theta
\end{cases}
$$

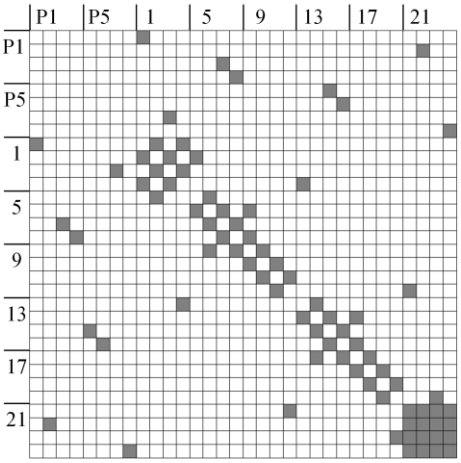

Fig. 10. Coupling matrix of the proposed filtering SPJ and the coupling values. Entries painted in grey are non-zero values. The values are given on the left.

$$
\begin{cases}
\angle S_{31} - \angle S_{32} = 0^\circ \\
\angle S_{41} - \angle S_{42} = 180^\circ \\
\angle S_{51} - \angle S_{52} = 270^\circ \\
\angle S_{61} - \angle S_{62} = 90^\circ
\end{cases} \tag{5}
$$

B. Coupling Matrix (CM) and Ideal Response

Coupling matrix (CM) [29] is widely used in the synthesis of filtering structures, but mostly based on resonant structures. However, the 90° 3-dB coupler (Fig. 7) used in the filtering SPJ is a non-resonant structure. To weave the structure into a CM, it must be represented by nodes. Previously in the design of an X-band filtering SPJ [23], a method of converting non-resonant components into CM representation was presented. (6) is the Y-matrix of the 90° 3-dB coupler shown in Fig. 8. Giving that, Fig. 7 was converted into a node-representation in Fig. 9, and the corresponding CM is given in Fig. 10.

$$
[Y_{90}] = j\sec 2\theta \begin{bmatrix}
-\sin 2\theta & \sqrt{2}\cos\theta & 1 & -\sqrt{2}\sin\theta \\
\sqrt{2}\cos\theta & -\sin 2\theta & -\sqrt{2}\sin\theta & 1 \\
1 & -\sqrt{2}\sin\theta & -\sin 2\theta & \sqrt{2}\cos\theta \\
-\sqrt{2}\sin\theta & 1 & \sqrt{2}\cos\theta & -\sin 2\theta
\end{bmatrix} \tag{6}
$$

The non-zero entries in Fig. 10 are painted in grey and their values are given. From the coupling matrix, the theoretical

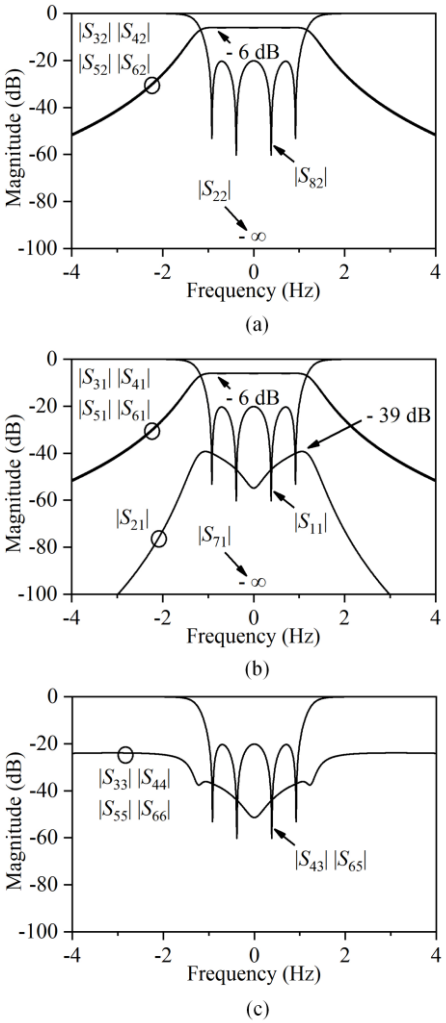

Fig. 11. Theoretical magnitude response of the filtering SPJ: (a) the response from Port 1; (b) the response from Port 2; and (c) the output response.

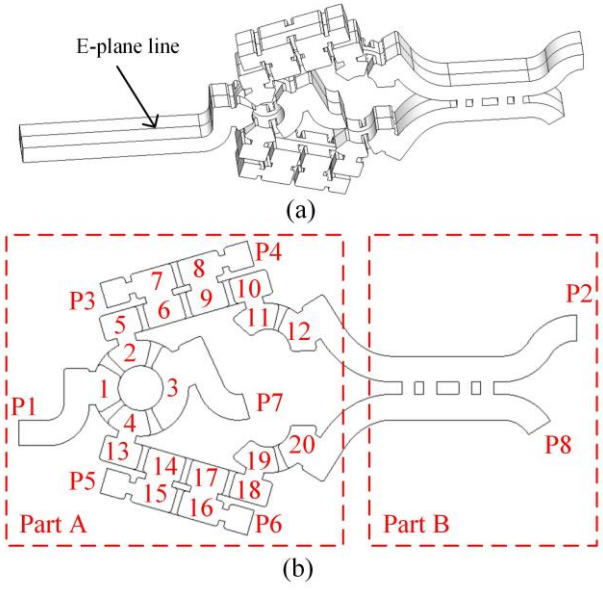

Fig. 12. Air model and the plan view of the proposed D-band E-plane filtering SPJ. (a) Overall view of the SPJ. The E-plane line is depicted as shown. (b) Front view. The resonators are numbered in red. Note Port 1 is shortened in (b) to make space for detail.

magnitude responses are deduced as shown in Fig. 11. Inheriting from the response of the filtering 90° coupler, $|S_{11}|$ and $|S_{82}|$ have a fourth-order Chebyshev response. The isolation between the two input ports (Port 1 and Port 2) is higher than 39 dB theoretically.

C. Realization of the D-Band E-Plane Filtering SPJ

The filtering SPJ was built in CST as an air model, using the 90° filtering coupler model at first, shown in Fig. 12, then fabricated using CNC machining. There are twenty resonators, all labelled with red numbers. The couplings to P3, P4, P5 and P6 are capacitive (to realize large couplings) while others are inductive. Resonators 1 to 4 are bent into a ring [30] to realize the E-plane structure with no capacitive iris. Resonator 11, 12, 19 and 20 are also bent. This is to make the upper and lower coupler more symmetrical and improve the output magnitude balance. Part B is the E-plane branch line coupler. P7 and P8 are to be loaded for better isolation and return loss. Fig. 13 provides the detail of the dimensions. The extension waveguide at each port was omitted for clarity.

D. Silicon-Chip Based Absorbers

P7 in the SPJ is inside the circuit periphery so it is difficult to connect to a separate waveguide load. To terminate it, we have designed and implemented a simple and compact load structure based on low-resistivity silicon chips. [31] and [32] used silicon as the absorber but with a complex shaped chip.

Fig. 14 shows the air model of our silicon chip absorber. It is simply formed of a slanted rectangular silicon substrate attached to the end of the waveguide. Two parameters determine its ability of absorption. One is the angle between the waveguide and the silicon chip, which is optimized to be 19.75° in this case. The other is the conductivity of the silicon chip

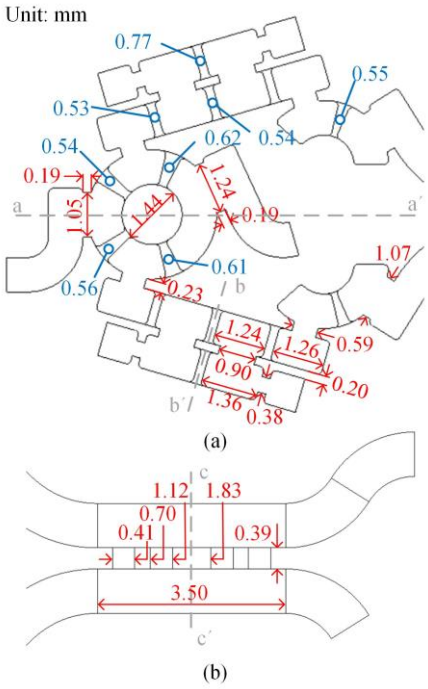

Fig. 13. Main dimensions of the SPJ. The dimensions along the E-plane are depicted in red while the ones along the H-planes are in blue. (a) Part A. Line aa' and line bb' are two symmetrical lines. (b) Part B. Line cc' is a symmetrical line.

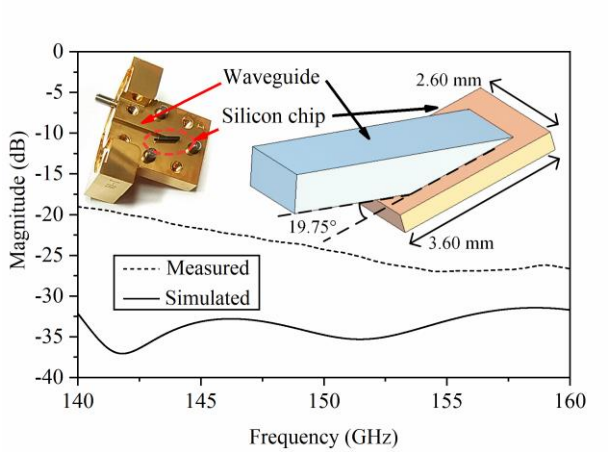

Fig. 14. Simulated and measured response of the matched load based on silicon chip absorber.

which is usually provided with a range of values. The estimated conductivity by measurement is around 12 S/m. The simulated and measured responses of the absorber are provided in Fig. 14. Simulated $|S_{11}|$ is lower than – 30 dB while measured one is lower than -20 dB in the shown frequency band. The discrepancy between measurement and simulation is partly due to the uncertainty in the silicon conductivity and partly due to assembly errors.

E. SPJ with Absorbers

The simulated magnitude responses of the filtering SPJ with silicon absorbers loaded are given in Fig. 15. It can be noticed, the return losses of the two inputs are higher than 20 dB in the working band. $|S_{21}|$, the isolation between the two inputs, is larger than 19 dB. Fig. 16 gives the simulated phase response of the filtering SPJ after having added the extension lines. In the

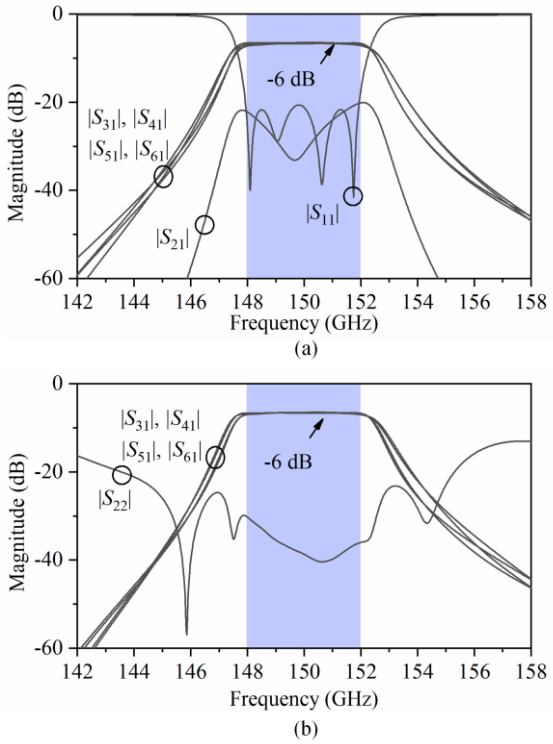

Fig. 15. Simulated magnitude response of the SPJ with two absorbers: (a) when input at Port 1; (b) when input at Port 2.

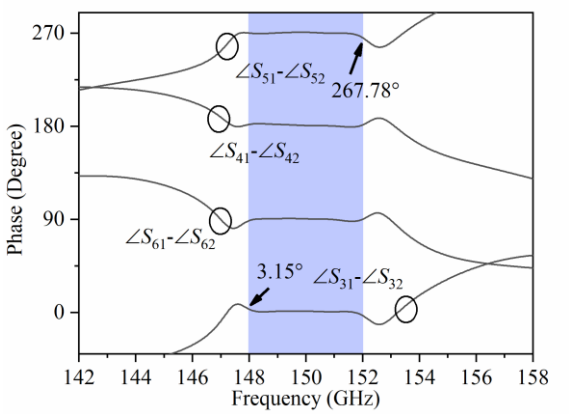

Fig. 16. Simulated phase response of the filtering SPJ with two absorbers.

working band, the phase values agree with (5), with a maximum in-band error of 3.2°.

IV. Fabrication and Measurement

The SPJ with slots for silicon chips (absorbers) was fabricated using CNC machining. The CAD model is given in Fig. 17. The device was separated along E-plane. The projected inside view is shown in Fig. 17(b). Extension lines were added to the ports to make space for flanges. There are two slots in Fig. 17(b) as marked out, reserved for silicon chips. The dimensions of the slots are given on the right side of Fig. 17(b). Their depth is 1.30 mm.

The CNC-machined model can be found in Fig. 18(a). Two silicon chips were loaded in the slots, zoomed in Fig. 18(b). The material is brass coated with gold. To measure the SPJ, four external loads were connected to the model, as shown in Fig. 19. Two of them are from the calibration kit and the other are in-house made using silicon chips (Fig. 14). The measurement setup can be found in Fig. 20. Four-port vector network analyzer (N5227A) was connected to two frequency extension modules (N5262AW06). The cables connecting to the LO port have a significant influence on the phase response. This was

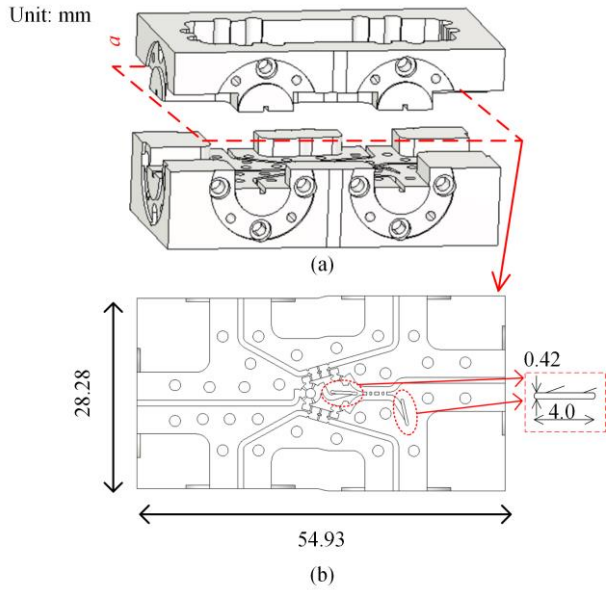

Fig. 17. CAD model of the filtering SPJ. (a) the two parts cut at E-plane. (b) the inside view of the model.

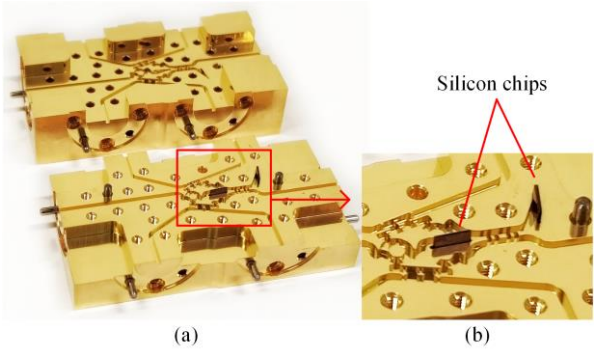

Fig. 18. Fabricated prototype of the filtering SPJ. (a) The overall view. (b) The zoomed-in viewgraph of the two silicon absorbers.

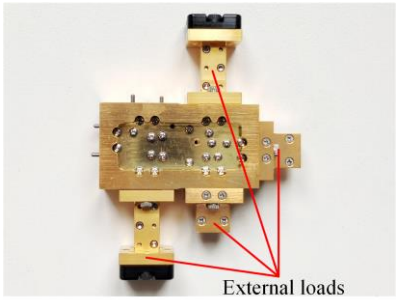

Fig. 19. Assembled SPJ with four external loads

minimized by using phase-stable cables and keeping them undisturbed [31]. The measured magnitude responses and phase response compared with simulated ones can be found in Fig. 21 and Fig. 22. The measured $|S_{11}|$ is lower than -11 dB in the working band. The measured in-band isolation between Port 1 and Port 2 is higher than 17.9 dB. Fig. 21(b) shows the measured magnitude response at Port 2. $|S_{22}|$ is below -20 dB in the working band. The maximum measured insertion loss at the four outputs at 150 GHz (center frequency) from the two inputs is 2.0 dB. The measured $|S_{11}|$ deviates more significantly from the simulation than others. This seems to indicate part of the circuit has larger manufacture errors than others. For instance, it is also observed that, for the S-parameters associated with Port 1, $|S_{31}|$ and $|S_{51}|$ show a larger insertion loss (maximum of 2 dB) than $|S_{41}|$ and $|S_{61}|$ (maximum of 0.5 dB). The phase response is in Fig. 22. The maximum in-band phase error in measurement is 15°. As each output of SPJ can be calibrated separately [5], the phase error is also acceptable.

Table I gives the comparison between the SPJs in the literature and this work. [23] is our previous work and [33] is another six-port junction integrated with the filtering function.

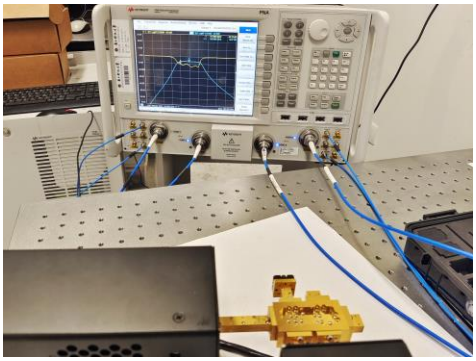

Fig. 20. Measurement setup of the SPJ.

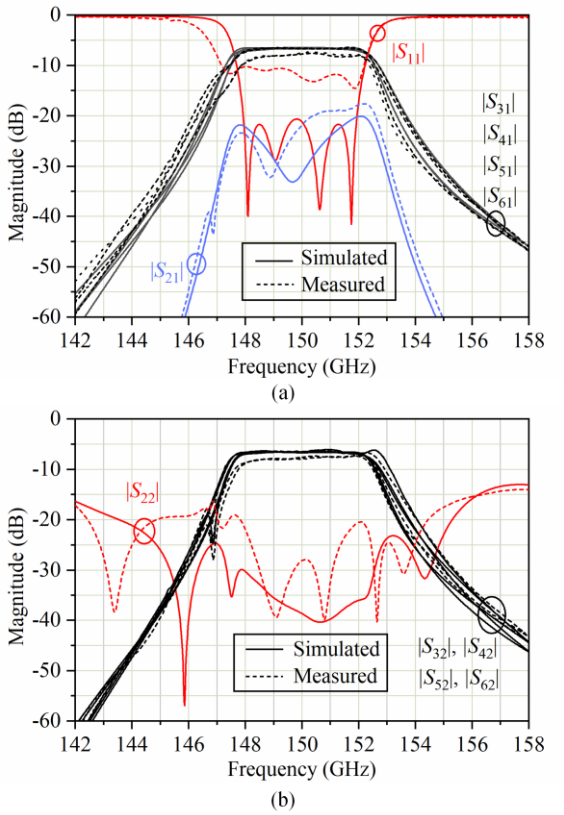

Fig. 21. Measured magnitude responses of the SPJ compared with simulated ones. (a) The response when input at Port 1. (b) When input at Port 2.

Compared with conventional SPJ using couplers and dividers, the resonator-based SPJ offers the integrated filtering function, which removes the need for additional external filters and the associated interconnection losses. This multi-pole resonator approach also provides more stable (or flatter) in-band magnitude as shown in Fig. 21.

V. Conclusion

An E-plane 90° filtering coupler and an E-plane filtering SPJ were presented in this work, both working in D band. There are ten resonators in the filtering coupler and twenty resonators in the filtering SPJ. This is one of the most complicated waveguide devices ever demonstrated in subterahertz frequency range. CM that combines resonant and non-resonant structures was used to synthesize the response of the SPJ.

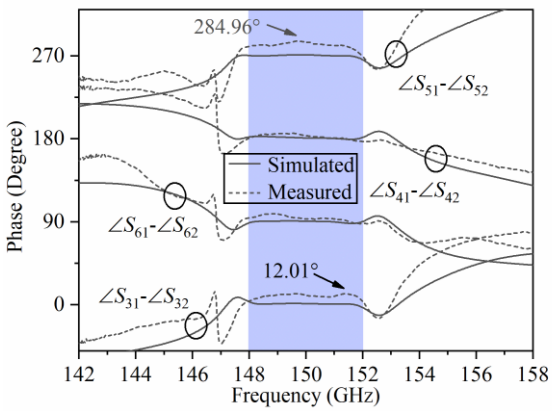

Fig. 22. Measured phase response.

TABLE I
Performance Comparison between SPJs

	f_0 (GHz)	IL (dB)	RL (dB)	ΔA (dB)	FBW	Iso. (dB)	FF
[6]	24	< 4.0	> 25	<5.0	16.7%	>21	/
[7]	30	< 2.2	> 13	<3.9	6.70%	>20	/
[23]	9.95	< 0.4	> 15	<0.5	4.02%	>26	√
[33]	7.75	< 1.9	> 21	<1.0	2.32%	>25	√
this work	150	< 2.0	> 11/> 20	<1.0	2.67%	>17.9	√

f_0 = center frequency, IL = insertion loss, RL = return loss, ΔA = amplitude imbalance, FBW = fractional bandwidth, Iso. = isolation between the two inputs. FF = filtering function.

Extremely large coupling values are required in the theoretical SPJ design to implement non-resonant nodes. Some infeasible coupling values were compromised in the practical design, still rendering the desired response. Also, two simple and compact silicon chips were employed as absorbers for the matched termination loads. Thanks to the implementation of the two 90° filtering coupler, all the ports in this SPJ was outside of the circuit compared with [23]. The measured response of the filtering SPJ shows no significant frequency shift compared with the simulation. The measurement shows the $|S_{11}|$ is lower than -11 dB and a $|S_{22}|$ lower than -20 dB. This is decent performance for a highly complex waveguide structure at 150 GHz. The maximum insertion loss at the center frequency (150 GHz) at the four output ports from the two input is 2.0 dB, which is higher than expected. This is most likely a result of the fabrication tolerance, which is 10 μm. The maximum phase error of the four outputs is 15° in the working band. The discrepancies manifested the challenge in manufacturing phase-sensitive waveguide devices at subterahertz frequency. Overall, for a passive signal distribution network as complex as this, the demonstrated performance is extremely encouraging and can be used in a subterahertz six-port receiver module.

The resonator-based SPJ benefits from the integrated filtering function and more stable in-band magnitude and phase over frequency. Compared with planar SPJ at similar frequency, the waveguide structure has the clear advantage in its low insertion loss. To form a SPJ mixer, Schottky-diode power detectors in waveguide housing can be connected to the four output ports. The scalability of production for subterahertz waveguide structures is indeed a challenge. Before this may be addressed eventually by microfabrication techniques such as silicon DRIE or micro-injection molding, the waveguide based six-port structure may be more suitable for small scale niche applications in instrumentation, radars and devices for space.

References

[1] W. R. Kincheloe and M. W Wilkens, "Phase and instantaneous frequency discriminator," United States Patent 3395346, Jul. 30, 1968.

[2] G. Engen and C. Hoer, "Application of an arbitrary 6-port junction to power-measurement problems", *IEEE Trans. Instrum. Meas.*, vol. IM-21, no. 4, pp. 470-474, Nov. 1972.

[3] Chang, K., *Encyclopedia of RF and Microwave Engineering*, New York: Wiley, 2005. pp. 3966-3977.

[4] T. Hentschel, "The six-port as a communications receiver", *IEEE Trans. Microw. Theory Tech.*, vol. 53, no. 3, pp. 1039-1047, Mar. 2005.

[5] A. Koelpin, G. Vinci, B. Laemmle, D. Kissinger and R. Weigel, "The six-port in modern society", *IEEE Microw. Mag.*, vol. 11, no. 7, pp. 35-43, Nov. 2010.

[6] Xinyu Xu, R. G. Bosisio and Ke Wu, "A new six-port junction based on substrate integrated waveguide technology," *IEEE Trans. on Microw. Theory Tech*., vol. 53, no. 7, pp. 2267-2273, Jul. 2005.

[7] A. A. Sakr, W. M. Dyab and K. Wu, "A dually polarized six-port junction based on polarization-selective coupling for polarization-inclusive remote sensing," *IEEE Trans. on Microw. Theory Tech.*, vol. 66, no. 8, pp. 3817-3827, Aug. 2018.

[8] F. Boccardi, R. W. Heath, Jr., A. Lozano, T. L. Marzetta, and P. Popovski, "Five disruptive technology directions for 5G," *IEEE Commun. Mag.*, vol. 52, no. 2, pp. 74–80, Feb. 2014.

[9] M. Cwiklinski et al., "D-band and G-Band high-performance GaN power amplifier MMICs," *IEEE Trans. Microw. Theory Techn.*, vol. 67, no. 12, pp. 5080–5089, Dec. 2019.

[10] P. J. Sobis, J. Stake and A. Emrich, "A 170 GHz 45° hybrid for submillimeter wave sideband separating subharmonic mixers," *IEEE Microw.Wireless Compon. Lett.*, vol. 18, no. 10, pp. 680-682, Oct. 2008.

[11] H. Rashid, D. Meledin, V. Desmaris and V. Belitsky, "Novel waveguide 3 dB hybrid with improved amplitude imbalance," *IEEE Microw.Wireless Compon. Lett.*, vol. 24, no. 4, pp. 212-214, Apr. 2014.

[12] Z. Niu et al., "A Novel 3-dB waveguide hybrid coupler for terahertz operation," *IEEE Microw. Wireless Compon. Lett.*, vol. 29, no. 4, pp. 273-275, Apr. 2019.

[13] H. Rashid, V. Desmaris, V. Belitsky, M. Ruf, T. Bednorz and A. Henkel, "Design of wideband waveguide hybrid with ultra-low amplitude imbalance," *IEEE Trans. THz Sci. Technol.*, vol. 6, no. 1, pp. 83-90, Jan. 2016.

[14] Z. Niu et al., "Mode analyzing method for fast design of branch waveguide coupler," *IEEE Trans. Microw. Theory Tech.*, vol. 67, no. 12, pp. 4733-4740, Dec. 2019.

[15] A. H. Khalil et al., "Quasi-elliptic and Chebyshev compact LTCC multipole filters functioning in the submillimetric wave region at 150 GHz," *IEEE Trans. Microw. Theory Techn*., vol. 58, no. 12, pp. 3925–3935, Dec. 2010.

[16] K. Wang, S.-W. Wong, G.-H. Sun, Z. Ning Chen, L. Zhu, and Q.-X. Chu, "Synthesis method for substrate-integrated waveguide bandpass filter with even-order Chebyshev response," *IEEE Trans. Compon. Packag. Manuf. Technol*., vol. 6, no. 1, pp. 126–135, Jan. 2016.

[17] S. W. Wong, K. Wang, Z.-N. Chen, and Q.-X. Chu, "Electric coupling structure of substrate integrated waveguide (SIW) for the application of 140-GHz bandpass filter on LTCC," *IEEE Trans. Compon. Packag. Manuf. Technol.*, vol. 4, no. 2, pp. 316–322, Feb. 2014.

[18] F. Lin, Q.-X. Chu, and S. W. Wong, "Design of dual-band filtering quadrature coupler using and resonators," *IEEE Microw. Wireless Compon. Lett.*, vol. 22, no. 11, pp. 565–567, Nov. 2012.

[19] M.-T. Chen and C.-W. Tang, "Design of the filtering power divider with a wide passband and stopband," *IEEE Microw. Wireless Compon. Lett.*, vol. 28, no. 7, pp. 570–572, Jul. 2018.

[20] W. J. Wu, Y. Z. Yin, S. L. Zuo, Z. Y. Zhang, and J. J. Xie, "A new compact filter-antenna for modern wireless communication systems," *IEEE Antennas Wireless Propag. Lett.*, vol. 10, pp. 1131–1134, Oct. 2011.

[21] S. J. Yang, Y. F. Cao, Y. M. Pan, Y. Wu, H. Hu and X. Y. Zhang, "Balun-Fed Dual-Polarized Broadband Filtering Antenna Without Extra Filtering Structure", *IEEE Antennas Wireless Propag. Lett.*, vol. 19, no. 4, pp. 656-660, Apr. 2020.

[22] Y. Li, Z. Zhao, Z. Tang, and Y. Yin, "Differentially fed, dual-band dual polarized filtering antenna with high selectivity for 5G sub-6 GHz base station applications," *IEEE Trans. Antennas Propag.*, vol. 68, no. 4, pp. 3231–3236, Apr. 2020.

[23] X. Chen, Y. Wang, T. Skaik and Q. Zhang, "E-Plane Waveguide Filtering Six-Port Junction," *IEEE Trans. Microw. Theory Techn*., vol. 69, no. 12, pp. 5360-5370, Oct. 2021.

[24] Y. J. Cheng, W. Hong and K. Wu, "Novel substrate integrated waveguide fixed phase shifter for 180-degree directional coupler," *IEEE MTT-S Int. Microw. Symp.*, Honolulu, HI, 2007, pp. 189-192.

[25] Q. Shao, F.-C. Chen, Q.-X. Chu and M. J. Lancaster, "Novel filtering 180° hybrid coupler and its application to 2×4 filtering butler matrix," *IEEE Trans. Microw. Theory Techn.*, vol. 66, no. 7, pp. 3288–3296, Jul. 2018.

[26] K. X. Wang, X. Liu, Y. C. Li, L. Z. Lin and X. Zhao, "LTCC filtering rat-race coupler based on eight-line spatially-symmetrical coupled Structure," *IEEE Access*, vol. 6, pp. 262-269, 2018.

[27] G. Zhang et al., "Compact single- and dual-band filtering 180° hybrid couplers on circular patch resonator," *IEEE Trans. Microw. Theory Techn.*, vol. 68, no. 9, pp. 3675-3685, Sep. 2020.

[28] W. Yu, Y. Rao, H. J. Qian and X. Luo, "Reflectionless filtering 90° coupler using stacked cross coupled-line and loaded cross-stub," *IEEE Microw. Wireless Compon. Lett.*, vol. 30, no. 5, pp. 481–484, May. 2020.

[29] R. J. Cameron, "Advanced coupling matrix synthesis techniques for microwave filters," *IEEE Trans. Microw. Theory Techn.*, vol. 51, no. 1, pp. 1-10, Jan. 2003.

[30] X. Chen, Y. Wang and Q. Zhang, "Ring-shaped D-band E-plane filtering coupler," in *IEEE Microw. and Wireless Compon. Lett.* vol. 31, no. 8, pp. 953-956, Aug. 2021.

[31] B. Beuerle, J. Campion, U. Shah and J. Oberhammer, "Integrated micromachined waveguide absorbers at 220–325 GHz," *Proc. 47th Eur. Microw. Conf. (EuMC), Nuremberg, Germany, Oct.* 2017, pp. 695-698.

[32] B. Beuerle, U. Shah and J. Oberhammer, "Micromachined Waveguides with Integrated Silicon Absorbers and Attenuators at 220–325 GHz," *IEEE MTT-S Int. Microw. Symp. Dig.*, Philadelphia, PA, USA, Jun. 2018, pp. 579-582.

[33] Y. J. Cheng and Y. Fan, "Compact substrate-integrated waveguide bandpass rat-race coupler and its microwave applications," *IET Microw. Antennas Propag.*, vol. 6, pp. 1000–1006, Sep. 2012.

Xun Chen was born in Chengdu, China. He received the B.Eng. and M.Eng. degree from University of Electronic Science and Technology of China, China, in 2015 and 2018, respectively. He is currently working toward the Ph.D. degree at University of Birmingham, UK and Southern University of Science and Technology, China. His research focuses on coupling matrix and passive devices, including diplexers, couplers and six-port junctions.

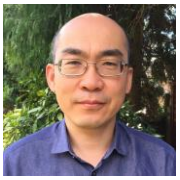

Yi Wang (M'09–SM'12) was born in Shandong, China. He received the B.Sc. degree in applied physics and M.Sc. degree in condensed matter physics from the University of Science and Technology, Beijing, China, in 1998 and 2001, respectively, and the Ph.D. degree in electronic and electrical engineering from the University of Birmingham, Edgbaston, Birmingham, U.K., in 2005.

From 2004 to 2011, he was a Research Fellow at the University of Birmingham. In 2011, he became a Senior Lecturer and then Reader at the University of Greenwich, U.K.. He is currently an Associate Professor with the University of Birmingham. He is the author of over 170 research papers. He has been the reviewer of several major microwave, antenna and sensor journals and an Associate Editor of IET MAP. He serves the TPC Chair of 2021 European Microwave Conference. His current research interests include multiport filtering networks, filter-antenna integration, millimeter-wave and terahertz antennas and devices for metrology, communication, and sensing. He is particularly interested in working with new materials and various novel manufacturing techniques, such as micromachining and 3D printing, for RF/microwave applications.

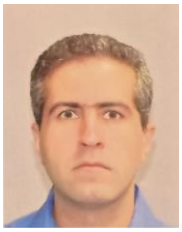

Milan Salek received the BEng degree in Electrical and Electronic Engineering from the Aston University, Birmingham, U.K., in 2016, and the Ph.D. degree in Microwave Engineering from the University of Birmingham, Birmingham, U.K., in 2019. Presently he is a Research Fellow in the Department of Electronic, Electrical and Systems Engineering, University of Birmingham. His current research interests include 3-D printed passive microwave devices, bolometric and diode-based power sensors, as well as millimeter-wave and terahertz circuits.

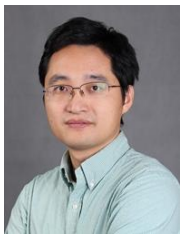

Qingfeng Zhang (Senior Member, IEEE) received the B.E. degree in electrical engineering from the University of Science and Technology of China (USTC), Hefei, China, in 2007, and the Ph.D. degree in electrical engineering from Nanyang Technological University, Singapore, in 2011.

From June 2011 to December 2013, he was a Post-Doctoral Fellow with the Poly-Grames Research Center, École Polytechnique de Montréal, Montreal, QC, Canada. Since December 2013, he has been with Southern University of Science and Technology (SUSTech), Shenzhen, China, where he is currently an Associate Professor with tenure. His research interests are largely in emerging novel electromagnetics technologies in which he has a special interest in dispersion engineering at microwave and millimeter-wave frequencies.

Dr. Zhang has served as a TPC member for various international conferences and on the review board of numerous journals in electromagnetics. He is also a fellow of the Institution of Engineering and Technology (IET). He received the URSI Young Scientist Award and the ACES Young Scientist Award in 2018. He is also the Vice-Chair of the IEEE Antennas and Propagation Society Shenzhen Chapter. He was the Publication Chair of the 2016 IEEE International Conference on Communication Systems (ICCS), the Local Organization Committee Co-Chair of 2017 IEEE Electrical Design of Advanced Packaging and Systems (EDAPS) Symposium, the TPC Co-Chair of Track 9 (Passive ICs and Active Antennas) in 2018 IEEE International Conference on Integrated Circuits, Technologies and Applications (ICTA), and the Track Chair of 2019 ComComAp. He has served as a Lead Guest Editor for the *International Journal of Antennas and Propagation* from 2014 to 2015. He has been serving as an Associate Editor for IEEE ACCESS since 2017.